Topological electronic structure and Weyl semimetal in the $TlBiSe_2$ class of semiconductors

Bahadur Singh,[1] Ashutosh Sharma,[1] H. Lin,[2,*] M. Z. Hasan,[3,4] R. Prasad,[1] and A. Bansil[2]
[1]*Department of Physics, Indian Institute of Technology Kanpur, Kanpur 208016, India*
[2]*Department of Physics, Northeastern University, Boston, Massachusetts 02115, USA*
[3]*Joseph Henry Laboratory, Department of Physics, Princeton University, Princeton, New Jersey 08544, USA*
[4]*Princeton Center for Complex Materials, Princeton University, Princeton, New Jersey 08544, USA*
(Received 27 June 2012; published 18 September 2012)

We present an analysis of bulk and surface electronic structures of thallium-based ternary III-V-VI_2 series of compounds $TlMQ_2$, where M = Bi or Sb and Q = S, Se, or Te, using the *ab initio* density functional theory framework. Based on parity analysis and (111) surface electronic structure, we predict $TlSbSe_2$, $TlSbTe_2$, $TlBiSe_2$, and $TlBiTe_2$ to be nontrivial topological insulators with a single Dirac cone at the Γ point and $TlSbS_2$ and $TlBiS_2$ to be trivial band insulators. Our predicted topological phases agree well with available angle-resolved photoemission spectroscopy measurements, in particular, the topological phase changes between $TlBiSe_2$ and $TlBiS_2$. Moreover, we propose that Weyl semimetal can be realized at the topological critical point in $TlBi(S_{1-x}Se_x)_2$ and $TlBi(S_{1-x}Te_x)_2$ alloys by breaking the inversion symmetry in the layer-by-layer growth in the order Tl-Se(Te)-Bi-S, yielding six Dirac cones centered along the Γ-*L* directions in the bulk band structure.

DOI: 10.1103/PhysRevB.86.115208 PACS number(s): 71.20.Nr, 71.15.Dx, 71.10.Pm, 73.20.At

I. INTRODUCTION

Topological insulators are a new class of materials which have attracted intense interest in the last few years[1–3] due to their exotic properties. These materials support an odd number of surface-state bands with a linear dispersion in the bulk energy gap, which can be viewed as a sea of massless Dirac fermions. The conducting surface states in topological insulators are protected by time-reversal symmetry and are immune to scattering by nonmagnetic impurities, thus opening new avenues for back-scattering-free transport. There also is a vigorous ongoing search for topological superconductors,[4,5] with the possibility of realizing Majorana fermions, which are their own antiparticles[6] with potential application to quantum computing.[7] Topological insulators have also generated considerable excitement due to the possibility of exploring the Higgs mechanism and realization of a Weyl semimetal in a condensed matter system.[8–13]

A topological phase was initially predicted in two-dimensional (2D) HgTe/CdTe quantum wells[14] and subsequently verified experimentally.[15] Soon thereafter a 2D conducting surface state was realized in the bulk band gap of the 3D thermoelectrics[16–18] $Bi_{1-x}Sb_x$, Bi_2Se_3, Bi_2Te_3, and Sb_2Te_3. However, magnetotransport studies[19–21] have shown that bulk transport dominates in these materials, motivating continued search for other 3D topological insulators with single-Dirac-cone surface states residing in the bulk energy gap. Since then first-principles calculations have suggested a large variety of topologically interesting materials, ranging from oxides[22] to the Heusler family of compounds.[23–25] Another class is thallium-based ternary III-V-VI_2 chalcogenides, which were proposed theoretically[26,27] and then verified experimentally.[28–30] These studies showed the existence of single-Dirac-cone-type surface states at the Γ point in $TlSbSe_2$, $TlSbTe_2$, $TlBiSe_2$, and $TlBiTe_2$. Also, it has been found that *p*-doped $TlBiTe_2$ superconducts,[31] where superconductivity is attributed to six leaf-like bulk pockets in the Fermi surface and the surface state becomes superconducting.[29]

Interestingly, recent studies[32,33] of $TlBi(S_{1-x}Se_x)_2$ alloys show that a topological phase transition can be realized by modulating either the spin-orbit coupling (SOC) or the crystal structure and that the surface Dirac fermion becomes massive at the quantum phase transition. This can be viewed as a condensed matter version of the Higgs mechanism in which a particle acquires a mass by spontaneous symmetry breaking. This system thus may provide a model system which connects condensed-matter physics to particle physics. It has also been proposed that a Weyl semimetal phase[34,35] could be achieved at the phase transition between a topological and a normal insulator if we explicitly break time-reversal symmetry[8,9] or inversion symmetry.[10,11] In this new phase, valence and conduction bands touch at certain points, called Weyl points, where dispersion is linear. These Weyl points come in pairs with positive and negative helicities and are robust to perturbations in the bulk material.

Our motivation for undertaking the present study is to provide a comprehensive investigation of the bulk and surface electronic structures of the thallium-based ternary III-V-VI_2 series of compounds $TlMQ_2$, where M = Bi or Sb and Q = S, Se, or Te, within a uniform first principles framework. In particular, not only the nontrivial compounds are studied,[36,37] but also the topologically trivial compound $TlBi(Sb)S_2$ is included since the recent angle-resolved photoemission spectroscopy (ARPES) measurement observed a topological phase transition in the alloy $TlBi(Se,S)_2$ between nontrivial $TlBiSe_2$ and trivial $TlBiS_2$.[33] We compare our theoretical predictions with the available ARPES results. Insight into the topological nature of these compounds is gained through slab computations in which the thickness of the slab is varied. Finally, the possibility of realizing a Weyl semimetal phase through strain in $TlBi(S_{1-x}Se_x)_2$ and $TlBi(S_{1-x}Te_x)_2$ alloys is examined for the first time, and it is shown that, when the inversion symmetry of the system is broken, a Weyl phase is indeed possible at the topological critical point where the system undergoes a transition from a trivial to a nontrivial (topological) insulator. Bulk and surface electronic structures of many members of the six ordered Tl compounds considered in this work have been discussed in several earlier papers in the literature.[26,27,36,37]

The organization of this article is as follows. Section II gives details of the bulk and surface computations. In Sec. III, we explain the bulk crystal structures, electronic structure, and parity analysis used to infer the topological nature of various compounds. Section IV discusses the slab structure used and relaxation and size-dependent effects. In Sec. V, we explain the topological phase transition and realization of the Weyl semimetal phase in $TlBi(S_{1-x}Se_x)_2$ and $TlBi(S_{1-x}Te_x)_2$ alloys. Section VI summarizes the conclusions of this study.

II. COMPUTATIONAL DETAILS

Electronic structure calculations were carried out within the framework of the density functional theory[38] using the VASP[39] (Vienna Ab Initio Simulation Package), with a projected augmented-wave basis.[40] Exchange-correlation effects were treated using a generalized gradient approximation[41] and SOC effects are included as implemented in the VASP. For structure optimization a plane-wave cutoff energy of 350 eV and a Γ-centered $8 \times 8 \times 8$ k mesh with the conjugate gradient algorithm[42] was used. Lattice parameters and ionic positions were adjusted until all components of Hellman-Feynman force on each ion were less than 0.001 eV/Å. Our surface electronic structure calculations are based on a slab geometry using bulk relaxed parameters with a net vacuum of 15 Å, a plane-wave cutoff energy of 350 eV, and a Γ-centered $9 \times 9 \times 1$ k mesh. Since ionic relaxations[36,37] are important, ionic positions in all slabs were optimized until the z component of the Hellman-Feynman forces was less than 0.005 eV/Å. Topological phase transition in $TlBi(S_{1-x}Se_x)_2$ and $TlBi(S_{1-x}Te_x)_2$ systems was investigated by taking the critical concentration of sulfur to be $x = 0.5$.[33]

III. RESULTS AND DISCUSSION

A. Bulk crystal structure

Thallium-based ternary chalcogenides III-V-VI_2 share a rhombohedral crystal structure [space group D^5_{3d} ($R\bar{3}\,m$)] with four atoms per unit cell, which occupy the Wyckoff positions 3a, 3b, and 6c.[43] We illustrate the crystal structure with the example of $TlBiTe_2$, which can be viewed as a distorted NaCl structure with four atoms in the primitive unit cell[43–45] and a sequence of hexagonal close-packed layers in the order Tl-Te-Bi-Te (see Fig. 1). The conventional unit cell is hexagonal and contains 12 atoms. The hexagonal lattice constants a_H and c_H can be computed from the rhombohedral parameters via the relation

$$a_H = 2a_R \sin\frac{\alpha}{2}, \quad c_H = a_R\sqrt{3 + 6\cos\alpha}, \tag{1}$$

where a_R is the rhombohedral lattice constant and α is the rhombohedral angle. Notably, the present compounds form a layered structure similar to that of binary topological insulators A_2B_3 (A = Bi or Sb and B = Se or Te),[16] where atoms are arranged in a sequence of five atomic layers or a quintuple repeating pattern. The bonding within the quintuple of layers is the ionic-covalent type, while between one quintuple group and the next it is the van der Waals type.[46] In order to gain insight into the nature of bonding in the thallium-based chalcogenides we have performed an electron localization function (ELF)[47] study, which shows that there is a negligible value of the ELF between the thallium and the tellurium layers, indicating predominantly ionic-type bonding between these layers. In contrast, the value of ELF between the bismuth and the tellurium layers is significant, implying ionic-covalent-type bonding. The optimized lattice and internal parameters u for the six Tl compounds considered are listed in Table I.

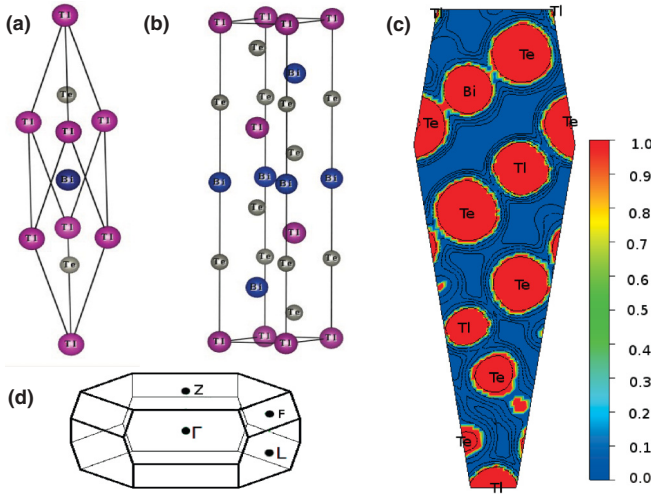

FIG. 1. (Color online) (a) Primitive and (b) conventional hexagonal crystal structure for $TlBiTe_2$. The conventional (hexagonal) unit cell has three times more atoms than the primitive cell. (c) ELF plot of $TlBiTe_2$ (see text). (d) Brillouin zone for the primitive unit cell with four time-reversal-invariant points, Γ, F, Z, and L.

B. Bulk band structures

The bulk band structures of $TlSbQ_2$ (Q = S, Se, and Te), shown in Fig. 2, indicate these three compounds to be narrow-gap semiconductors. $TlSbSe_2$ is seen to be a direct band-gap semiconductor with the valence band maximum (VBM) and conduction band minimum (CBM) lying along Γ-L. Here the SOC plays an important role, as it induces a band inversion at Γ, suggesting a possible nontrivial topological phase, a point to which we return below. $TlSbTe_2$ and $TlSbS_2$ are also shown in Figs. 2(b) and 2(c) to be direct band-gap semiconductors with the VBM and CBM at the Γ point. Since Te is heavier than Se, there is a large SOC effect in $TlSbTe_2$. But the S atom is lighter than Se and Te so that SOC effects are smaller in $TlSbS_2$.

The bulk band structures of $TlBiQ_2$ (Q = Se, Te, and S) are shown in Fig. 3. There is a large effect of SOC

TABLE I. Optimized lattice constant a_R, angle α, and internal parameter u for six thallium-based rhombohedral compounds.

Compound	a_R (Å)	α (deg)	u
$TlSbSe_2$	7.955	30.869	0.2374
$TlSbTe_2$	8.421	31.367	0.2386
$TlSbS_2$	7.718	30.568	0.2352
$TlBiSe_2$	7.989	31.368	0.2391
$TlBiTe_2$	8.367	31.847	0.2413
$TlBiS_2$	7.979	29.764	0.2368

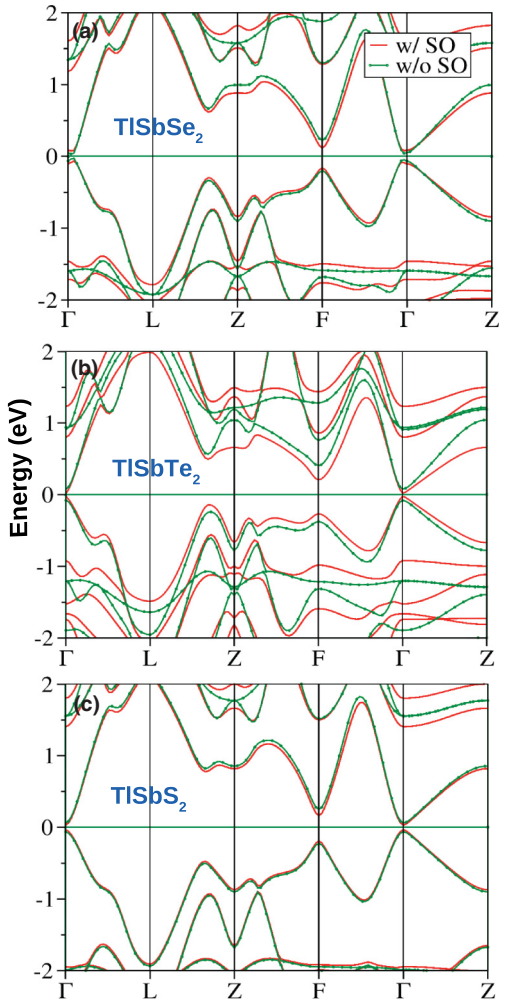

FIG. 2. (Color online) Bulk band structures of rhombohedral (a) $TlSbSe_2$, (b) $TlSbTe_2$, and (c) $TlSbS_2$ along high-symmetry lines with (red lines) and without (green lines) spin-orbit coupling (SO).

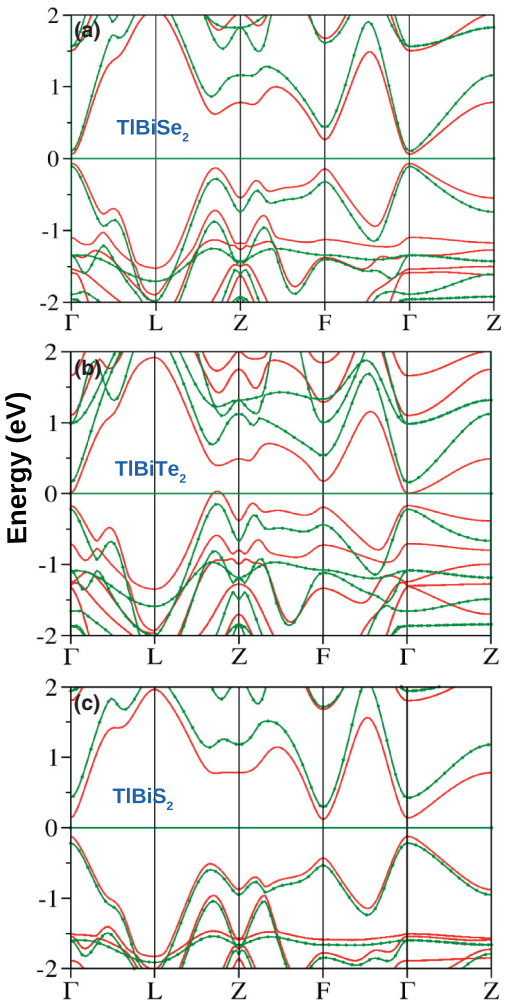

FIG. 3. (Color online) Bulk band structures of rhombohedral (a) $TlBiSe_2$, (b) $TlBiTe_2$, and (c) $TlBiS_2$ along the high-symmetry line with (red lines) and without (green lines) spin-orbit coupling.

due to the presence of the heavier Bi atom. Our band structures agree well with an earlier study,[45] except in the case of $TlBiTe_2$, which was previously found to be[45] an indirect gap semiconductor with the VBM lying along the L-Z direction and the CBM at the Γ point. However, for our relaxed structure (including SOC) the VBM and CVM still lie at the aforementioned $\vec{k}$ points, but the system is semimetallic with a band gap of -10 meV. This is in accord with the corresponding experimental results,[29] which found the material to be semimetallic with a band gap of -20 meV.

C. Parity analysis

Since all the investigated compounds possess inversion symmetry, a parity analysis[48] can be used to identify the Z_2 topological phases. There are eight time-reversal-invariant points in the rhombohedral Brillouin zone, but only four points [Γ, F, L, and Z; see Fig. 1(d)] are inequivalent. Products of parity eigenvalues at these four momenta are listed in Table II with and without SOC.

Table II shows that the product of parity eigenvalues in $TlBiSe_2$, $TlBiTe_2$, $TlSbSe_2$, and $TlSbTe_2$ changes at Γ as SOC is turned on, yielding a nontrivial topological-invariant $Z_2 = 1$. The nontrivial topological character of these compounds is thus due to band inversion at the Γ point.[26,27,36] On the other hand, there is no band inversion for $TlSbS_2$ and $TlBiS_2$ at any of the time-reversal-invariant momenta, indicating that these compounds are topologically trivial.

TABLE II. Products of parity eigenvalues at the four inequivalent time-reversal-invariant k points in the six investigated compounds. wso, without spin-orbit coupling; so, with spin-orbit coupling.

	Γ × 1		L × 3		F × 3		Z × 1		
Compound	wso	so	wso	so	wso	so	wso	so	Z_2
$TlSbSe_2$	+	−	+	+	+	+	+	+	1
$TlSbTe_2$	+	−	+	+	+	+	+	+	1
$TlSbS_2$	+	+	+	+	+	+	+	+	0
$TlBiSe_2$	+	−	+	+	+	+	+	+	1
$TlBiTe_2$	+	−	+	+	+	+	+	+	1
$TlBiS_2$	+	+	+	+	+	+	+	+	0

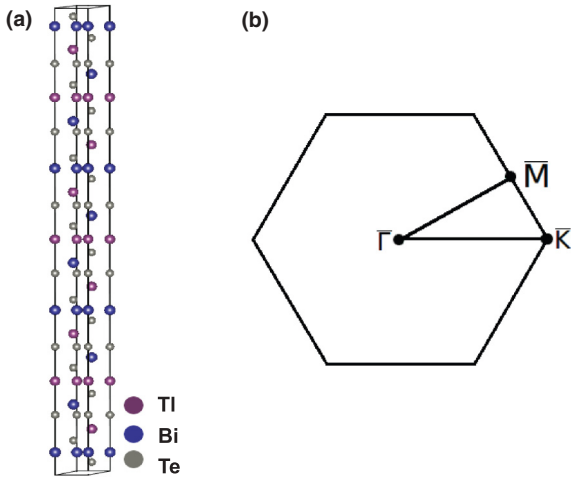

FIG. 4. (Color online) (a) Structure of a 39-atomic-layer slab of $TlBiTe_2$ stacked along the z direction. (b) 2D Brillouin zone with three special k points, $\bar{\Gamma}$, $\bar{M}$, and $\bar{K}$.

IV. SURFACE ANALYSIS

A. Slab structure and relaxation

A hexagonal unit cell is used for all slab computations, with atomic layers stacked in the z direction. Since atoms along the z direction are sequenced in the order Tl-Te(S, Se)-Bi(Sb)-Te(S, Se), there are four possible surface terminations, depending on which atom lies in the topmost layer. The bond length between Tl and Te is large ($d = 350$ pm), whereas the bond length between Bi and Te is small ($d = 318$ pm). Thus, of the four possible surface terminations, we have used the one with the Q (Se, Te, and S) atom at the surface and Bi (Sb) under it in the second layer, as this termination has a minimum number of dangling bonds.[26] Optimized bulk parameters were used to construct slabs of different thicknesses. A symmetric 39-atomic-layer slab of $TlBiTe_2$ and the associated surface Brillouin zone are shown in Fig. 4. Surface relaxation is known to play an important role,[36,37] and accordingly, we have relaxed all atomic layers in the slabs used, although the relaxation effect is small as we move into the bulk.

B. $TlSbQ_2$ (Q = Se, Te, or S)

The Q-atom-terminated surface electronic structures of the three compounds are shown in Fig. 5 for different slab thicknesses together with the associated projected bulk bands (aqua region). Figures 5(a) and 5(b) show the surface band structure of $TlSbSe_2$ for slabs of 35 (thickness ≈ 6.4 nm) and 47 (thickness ≈ 8.6 nm) layers, respectively. In the 35-layer slab there is a band gap of 50 meV at the $\bar{\Gamma}$ point. As the number of layers increases, the size of the gap decreases. For 47 layers, this gap is negligible and we get a clear Dirac-cone surface state in the bulk gap region. Moreover, around −0.8 eV we obtain a Rasbha-type, trivial-spin split surface state in both slabs.[36] Figure 5(c) shows results for a 47-layer $TlSbTe_2$ slab, which are similar to those for $TlSbSe_2$. Finally, $TlSbS_2$ does not display any metallic surface state, which confirms its topologically trivial nature.

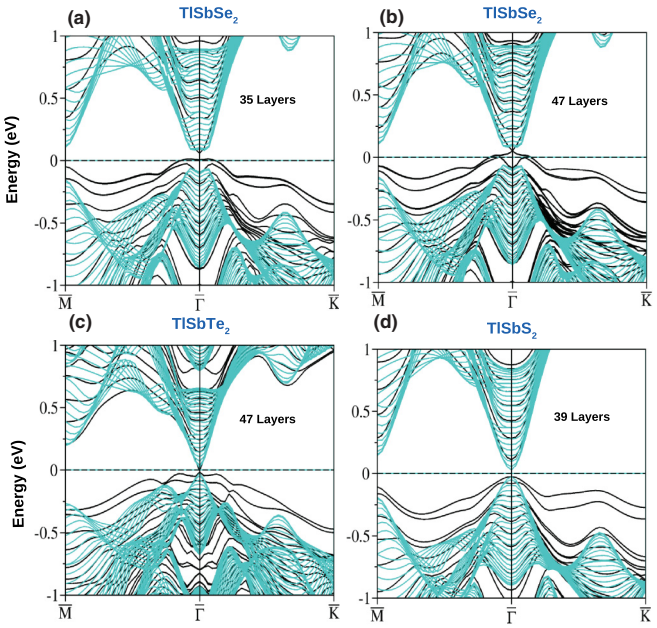

FIG. 5. (Color online) Surface electronic structure of various slabs: (a) 35-layer (≈6.4-nm) $TlSbSe_2$; (b) 47-layer (≈8.6-nm) $TlSbSe_2$; (c) 47-layer (≈9.2-nm) $TlSbTe_2$; and (d) 39-layer (≈6.9-nm) $TlSbS_2$, along high-symmetry lines in the surface Brillouin zone. Bulk bands projected on the surface Brillouin zone are shown in aqua.

C. $TlBiQ_2$ (Q = Se, Te, or S)

Similarly to $TlSbQ_2$, $TlBiQ_2$ also shows a thickness-dependent slab electronic structure. Figure 6 shows the surface band structure of $TlBiSe_2$. With a slab thickness of ≈6.3 nm we get a gapped surface state with a gap of 36 meV, and as

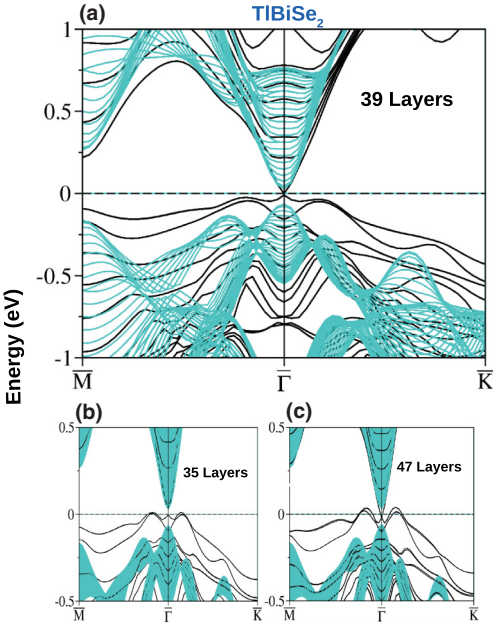

FIG. 6. (Color online) Surface electronic structure of various slabs: (a) 39-layer (≈7.0-nm) $TlBiSe_2$; (b) 35-layer (≈6.3-nm) $TlBiSe_2$; and (c) 47-layer (≈8.7-nm) $TlBiSe_2$, along high-symmetry lines in the surface Brillouin zone. Projected bulk bands are shown in aqua.

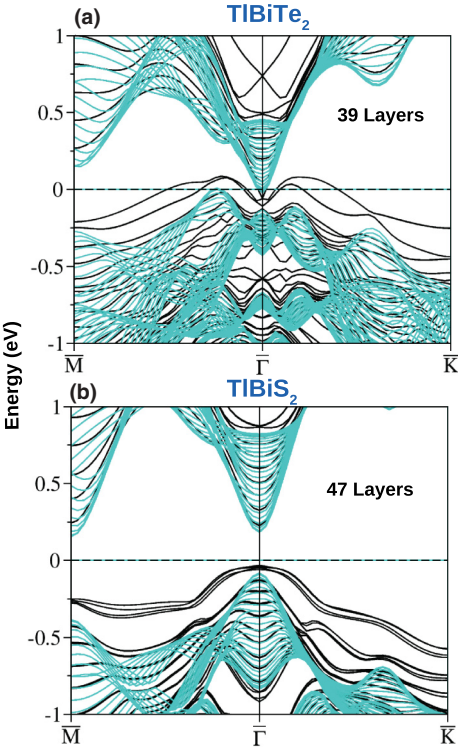

FIG. 7. (Color online) Surface electronic structure of (a) a 39-layer (≈7.4-nm) $TlBiTe_2$ slab and (b) a 47-layer (≈8.6-nm) $TlBiS_2$ slab, along high-symmetry lines in the surface Brillouin zone. The aqua color shows projected bulk bands.

we increase the slab thickness to ≈7.0 nm this gap decreases to 9 meV. The gap at a small slab thickness arises due to interaction between the opposite faces of the slab. As we increase the slab thickness further, to ≈8.7 and ≈10.9 nm, we obtain a clear Dirac state with a negligible gap. At a critical thickness of ≈7.0 nm the Dirac point is isolated, i.e., no other states are at the energy of the Dirac point, which agrees with recent ARPES[28–30] measurements. The observed Dirac state for slabs thicker than 7.0 nm is surrounded by the surface bands, which is somewhat different from ARPES results and requires further study.

Figure 7(a) shows results for $TlBiTe_2$, which exhibits a Dirac-like surface state in the bulk gap region at a thickness of ≈7.4 nm (39 layers). The Dirac point lies 0.1 eV below the Fermi energy, in accord with ARPES studies.[29] The electronic structure displays an indirect band gap near the $\bar{\Gamma}$ point, with the bulk CBM at the $\bar{\Gamma}$ point and bulk valence band maxima along the $\bar{\Gamma}$-$\bar{M}$ and $\bar{\Gamma}$-$\bar{K}$ directions. The location of the Dirac point in our calculation is close to experimental results, where the Dirac point lies 0.3 eV below the Fermi energy. Results for $TlBiS_2$ in Fig. 7(b) do not have any metallic surface state in the bulk gap region, indicating its topologically trivial character.

V. TOPOLOGICAL PHASE TRANSITION AND WEYL SEMIMETAL

A. $TlBi(S_{1-x}Se_x)_2$

A topological phase transition was observed in $TlBi(S_{1-x}Se_x)_2$ in which the S and Se atoms are disordered

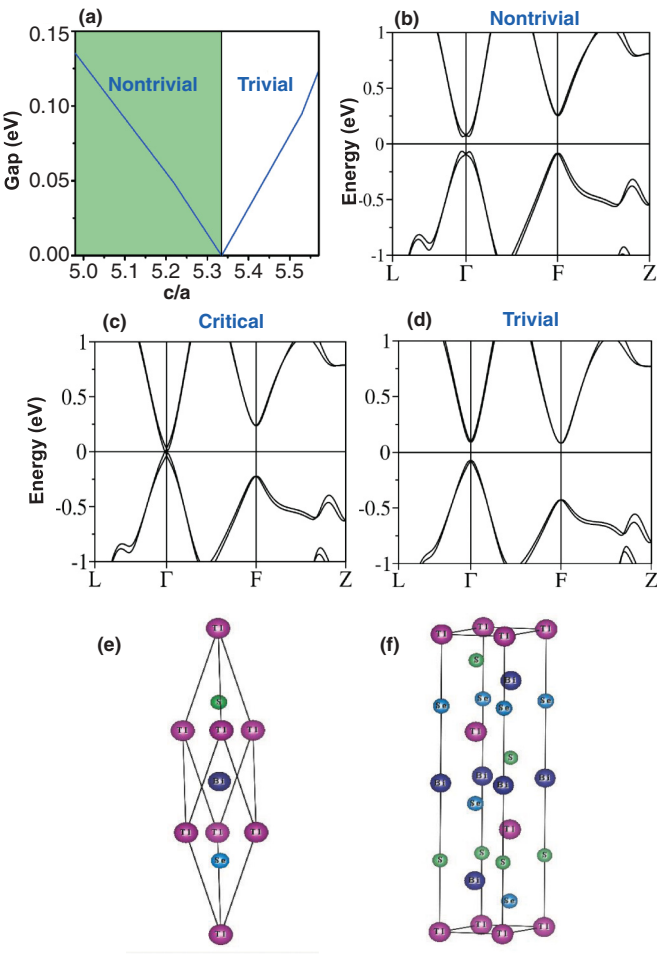

FIG. 8. (Color online) (a) Phase diagram for the topological phase transition. The system is tuned from a normal to a topological insulator by changing the c/a ratio. (b–d) Bulk band structure of TlBiSeS for (b) $c/a = 5.22$, (c) $c/a = 5.33$, and (d) $c/a = 5.58$. (e) Primitive rhombohedral and (f) conventional hexagonal crystal structure for TlBiSeS. The layered structure is with no inversion symmetry.

and inversion symmetry is preserved on average with the inversion center at the (Se,S) site.[33] At the critical composition $x \sim 0.5$, the conduction and valence bands meet at the Γ point and form 3 + 1D Dirac-cone bulk states. The Dirac-cone states are doubly degenerate due to inversion and time-reversal symmetries. When the inversion symmetry is broken, the spin degeneracy can be lifted. Here we consider an ordered phase of TlBiSSe with layers in the order Tl-Se-Bi-S as shown in Figs. 8(e) and 8(f). The inversion symmetry is now seen to be broken, as Se and S sites are no longer inversion centers. Our theoretical fully relaxed structure, which is rhombohedral, is found to be stable, indicating that the material should be possible to realize via molecular beam epitaxy techniques. In the absence of inversion symmetry, parity analysis cannot be applied to delineate the topological nature, but adiabatic continuity arguments can be used. Accordingly, we start from a normal insulator with a large value of c/a and systematically reduce its value. During this process the system passes from a normal to a topological insulator as shown in Fig. 8(a). The

band structure for the normal and topological phase through the critical point is shown in Figs. 8(b)–8(d). The critical point occurs when the gap closes. At $c/a = 4.98$, the band gap is 0.135 eV, and the bulk valence band has no s character, while the bulk conduction band possesses a finite s character at Γ. These characteristic symmetries are the same as in $TlBiSe_2$, indicating that the two compounds are adiabatically connected and are thus both topologically nontrivial. With increasing c/a value the gap decreases and becomes 0 at the critical value $c/a = 5.33$. Upon further increasing c/a, the bulk gap increases and becomes 0.129 eV at $c/a = 5.58$, and the bulk valence and conduction bands swap their orbital character at the Γ point. The system is now adiabatically connected to $TlBiS_2$ and is, therefore, topologically trivial.

Interestingly, at the topological critical point, the band gap at Γ remains finite, with a value of 0.062 eV. However, the band gap closes along Γ-L at $\vec{k} = (0.0, 0.0, 0.007)$. Thus, by breaking the inversion symmetry, we obtain a nondegenerate spin-polarized bulk Dirac cone, instead of the doubly degenerate Dirac cone found in Se/S disordered $TlBi(Se,S)_2$. The bulk valence and conduction bands now touch each other and display linear dispersion, which can be described by a two-component wave function, i.e. by the Weyl equation. A Weyl semimetal is formed at the critical point, with six Weyl points centered along Γ-L.[49] The detailed band structure is shown in Fig. 9.

B. $TlBi(S_{1-x}Te_x)_2$

Analysis of $TlBi(S_{1-x}Te_x)_2$ follows along the lines of that of $TlBi(S_{1-x}Se_x)_2$ in the preceding subsection, and therefore, we only make a few relevant remarks. Here again we take the critical point to be at $x = 0.5$, break the inversion symmetry by considering an ordered phase with layers in the sequence Tl-Te-Bi-S, and compute the band structure for a series of c/a values. The results, summarized in Fig. 10, show that at $c/a = 4.93$ there is a direct band gap of 0.123 eV along Γ-L, although there is an indirect gap of ≈10 meV. At the critical value of $c/a = 5.00$, the gap becomes 0 along Γ-L at $\vec{k} = (0.0, 0.0, 0.025)$, even though the gap remains finite at Γ, with a value of 0.210 eV. With a further increase in c/a, the gap reopens and becomes 0.221 eV at $c/a = 5.57$. Adiabatic continuity arguments combined with the change in the orbital character of the bulk valence and conduction bands at the critical value of c/a then allow us to conclude the nontrivial-to-trivial insulator transition shown in Fig. 10(a). As for the Weyl semimetal phase, at the critical c/a value, $TlBi(S_{1-x}Te_x)_2$ displays six

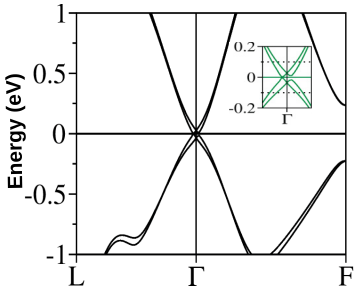

FIG. 9. (Color online) Band dispersion at the critical point in $TlBi(S_{1-x}Se_x)_2$. Inset: Dispersion near the Γ point.

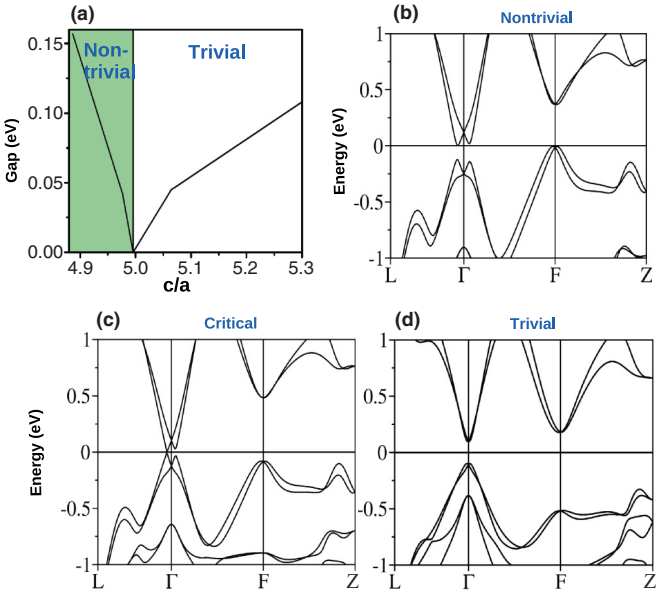

FIG. 10. (Color online) (a) Phase diagram of topological phase transition in TlBiTeS. (b–d) Bulk band structure of TlBiTeS for $c/a = 4.93$, $c/a = 5.00$, and $c/a = 5.57$.

Weyl points along the Γ-L direction, at $\vec{k} = (0.0, 0.0, 0.025)$, although the spin splitting is larger than in $TlBi(S_{1-x}Se_x)_2$.

VI. CONCLUSIONS

We have carried out an *ab initio* study of bulk and surface electronic structures of six thallium-based III-V-VI_2 ternary chalcogenides $TlMQ_2$, where M = Bi or Sb and Q = S, Se, or Te, with the focus on delineating the topological nature of these compounds. $TlBiTe_2$ is found to be a semimetal with a band gap of −10 meV, while the other five Tl compounds are all small-band-gap semiconductors. Based on an analysis of parities of bulk band structures, we predict that $TlSbSe_2$, $TlSbTe_2$, $TlBiSe_2$, and $TlBiTe_2$ are nontrivial topological insulators with band inversion at the Γ point, but $TlSbS_2$ and $TlBiS_2$ are trivial band insulators. Moreover, surface-state computations show that the surface Dirac states lie in the gap region at the Γ point in all four aforementioned topological compounds. Our predicted topological phases and the Γ point centered Dirac-cone surface states are in substantial accord with available ARPES results. Electronic structures of slabs with different numbers of layers were computed in order to gain insight into thickness-dependent effects. The gap opens at the Dirac point for thin slabs and decreases with increasing thickness. Finally, we investigated $TlBi(S_{1-x}Se_x)_2$ and $TlBi(S_{1-x}Te_x)_2$ alloys for $x = 0.5$, where the inversion symmetry was explicitly broken by using layers in the sequence Tl-Se(Te)-Bi-S and the c/a ratio was varied. Both alloys were found to undergo a topological transition at a critical value of c/a at which the spin degeneracy of the Dirac states is lifted and a Weyl semimetal phase can be realized with six Weyl points in the bulk Brillouin zone located along the Γ-L directions.

ACKNOWLEDGMENTS

We thank Diptiman Sen for helpful discussions. The work was supported by the Department of Science and Technology, New Delhi (India), through Project No. SR/S2/CMP-0098/2010 and US Department of Energy, Office of Science, Basic Energy Sciences Contract No. DE-FG02-07ER46352 and benefited from the allocation of supercomputer time at NERSC and Northeastern University's Advanced Scientific Computation Center (ASCC). M.Z.H. is supported by the Office of Basic Energy Sciences, US Department of Energy Grant No. DE-FG-02-05ER46200 and the A. P. Sloan Foundation Fellowship.

*Corresponding author: nilnish@gmail.com

[1] X.-L. Qi and S.-C. Zhang, Phys. Today **63**, 33 (2010).
[2] M. Z. Hasan and C. L. Kane, Rev. Mod. Phys. **82**, 3045 (2010).
[3] M. Z. Hasan and J. E. Moore, Ann. Rev. Cond. Mat. Phys. **2**, 55 (2011).
[4] X.-L. Qi, T. L. Hughes, S. Raghu, and S.-C. Zhang, Phys. Rev. Lett. **102**, 187001 (2009).
[5] A. P. Schnyder, S. Ryu, A. Furusaki, and A. W. W. Ludwig, Phys. Rev. B **78**, 195125 (2008).
[6] F. Wilczek, Nat. Phys. **5**, 614 (2009).
[7] C. Nayak, S. H. Simon, A. Stern, M. Freedman, and S. Das Sarma, Rev. Mod. Phys. **80**, 1083 (2008).
[8] X. Wan, A. M. Turner, A. Vishwanath, and S. Y. Savrasov, Phys. Rev. B **83**, 205101 (2011).
[9] A. A. Burkov and L. Balents, Phys. Rev. Lett. **107**, 127205 (2011).
[10] G. B. Halász and L. Balents, Phys. Rev. B **85**, 035103 (2012).
[11] S. Murakami, S. Iso, Y. Avishai, M. Onoda, and N. Nagaosa, Phys. Rev. B **76**, 205304 (2007).
[12] K.-Y. Yang, Y.-M. Lu, and Y. Ran, Phys. Rev. B **84**, 075129 (2011).
[13] S. M. Young, S. Zaheer, J. C. Y. Teo, C. L. Kane, E. J. Mele, and A. M. Rappe, Phys. Rev. Lett. **108**, 140405 (2012).
[14] B. A. Bernevig, T. L. Hughes, and S.-C. Zhang, Science **314**, 1757 (2006).
[15] M. König, H. Buhmann, L. W. Molenkamp, T. Hughes, C.-X. Liu, X.-L. Qi, and S.-C. Zhang, J. Phys. Soc. Jpn. **77**, 031007 (2008).
[16] H. Zhang, C.-X. Liu, X.-L. Qi, X. Dai, Z. Fang, and S.-C. Zhang, Nat. Phys. **5**, 438 (2009).
[17] D. Hsieh, D. Qian, L. Wray, Y. Xia, Y. S. Hor, R. J. Cava, and M. Z. Hasan, Nature **452**, 970 (2008).
[18] Y. Xia, D. Qian, D. Hsieh, L. Wray, A. Pal, H. Lin, A. Bansil, D. Grauer, Y. S. Hor, R. J. Cava, and M. Z. Hasan, Nat. Phys. **5**, 398 (2009).
[19] J. G. Analytis, J.-H. Chu, Y. Chen, F. Corredor, R. D. McDonald, Z. X. Shen, and I. R. Fisher, Phys. Rev. B **81**, 205407 (2010).
[20] K. Eto, Z. Ren, A. A. Taskin, K. Segawa, and Y. Ando, Phys. Rev. B **81**, 195309 (2010).
[21] N. P. Butch, K. Kirshenbaum, P. Syers, A. B. Sushkov, G. S. Jenkins, H. D. Drew, and J. Paglione, Phys. Rev. B **81**, 241301(R) (2010).
[22] A. Shitade, H. Katsura, J. Kunes, X.-L. Qi, S.-C. Zhang, and N. Nagaosa, Phys. Rev. Lett. **102**, 256403 (2009).
[23] H. Lin, L. A. Wray, Y. Xia, S. Xu, S. Jia, R. J. Cava, A. Bansil, and M. Z. Hasan, Nat. Mater. **9**, 546 (2010).
[24] S. Chadov, X. Qi, Jürgen Kübler, G. H. Fecher, C. Felser, and S. C. Zhang, Nat. Mater. **9**, 541 (2010).
[25] M. Franz, Nat. Mater. **9**, 536 (2010).
[26] H. Lin, R. S. Markiewicz, L. A. Wray, L. Fu, M. Z. Hasan, and A. Bansil, Phys. Rev. Lett. **105**, 036404 (2010).
[27] B. Yan, C.-X. Liu, H.-J. Zhang, C.-Y. Yam, X.-L. Qi, T. Frauenheim, and S.-C. Zhang, Europhys. Lett. **90**, 37002 (2010).
[28] K. Kuroda, M. Ye, A. Kimura, S. V. Eremeev, E. E. Krasovskii, E. V. Chulkov, Y. Ueda, K. Miyamoto, T. Okuda, K. Shimada, H. Namatame, and M. Taniguchi, Phys. Rev. Lett. **105**, 146801 (2010).
[29] Y. L. Chen, Z. K. Liu, J. G. Analytis, J.-H. Chu, H. J. Zhang, B. H. Yan, S.-K. Mo, R. G. Moore, D. H. Lu, I. R. Fisher, S. C. Zhang, Z. Hussain, and Z.-X. Shen, Phys. Rev. Lett. **105**, 266401 (2010).
[30] T. Sato, K. Segawa, H. Guo, K. Sugawara, S. Souma, T. Takahashi, and Y. Ando, Phys. Rev. Lett. **105**, 136802 (2010).
[31] R. A. Hein and E. M. Swiggard, Phys. Rev. Lett. **24**, 53 (1970).
[32] T. Sato, K. Segawa, K. Kosaka, S. Souma, K. Nakayama, K. Eto, T. Minami, Y. Ando, and T. Takahashi, Nat. Phys. **7**, 840 (2011).
[33] S.-Y. Xu, Y. Xia, L. A. Wray, S. Jia, F. Meier, J. H. Dil, J. Osterwalder, B. Slomski, A. Bansil, H. Lin, R. J. Cava, and M. Z. Hasan, Science **332**, 560 (2011).
[34] H. Nielsen and M. Ninomiya, Phys. Lett. B **130**, 389 (1983).
[35] H. B. Nielsen and M. Ninomiya, Nucl. Phys. B **185**, 20 (1981).
[36] S. V. Eremeev, G. Bihlmayer, M. Vergniory, Y. M. Koroteev, T. V. Menshikova, J. Henk, A. Ernst, and E. V. Chulkov, Phys. Rev. B **83**, 205129 (2011).
[37] J. Chang, L. F. Register, S. K. Banerjee, and B. Sahu, Phys. Rev. B **83**, 235108 (2011).
[38] P. Hohenberg and W. Kohn, Phys. Rev. **136**, B864 (1964).
[39] G. Kresse and J. Furthmüller, Phys. Rev. B **54**, 11169 (1996).
[40] G. Kresse and D. Joubert, Phys. Rev. B **59**, 1758 (1999).
[41] J. P. Perdew, K. Burke, and M. Ernzerhof, Phys. Rev. Lett. **77**, 3865 (1996).
[42] W. H. Press, B. P. Flannery, S. A. Teukolsky, and W. T. Vetterling, *Numerical Recipes* (Cambridge University Press, New York, 1986).
[43] E. F. Hockings and J. G. White, Acta Crystallogr. **14**, 328 (1961).
[44] O. Madelung, *Semiconductors: Data Handbook*, 3rd ed. (Springer-Verlag, Berlin, 2004).
[45] K. Hoang and S. D. Mahanti, Phys. Rev. B **77**, 205107 (2008).
[46] S. Satpathy, S. K. Mishra, and O. Jepsen, Condens. Matter **9**, 461 (1997).
[47] R. Nesper, S. Wengert, A. Savin, and T. E. Fassler, Angew. Chem. Int. Ed. Engl. **36**, 1808 (1997).
[48] L. Fu and C. L. Kane, Phys. Rev. B **76**, 045302 (2007).
[49] A topologically protected Weyl semimetal phase can be realized by removing the rotation symmetry of the crystal. The gapless semimetal phase is then stable over a finite region of a tuning parameter.